Rapid evolutionary repair by secondary perturbation of a primary disrupted transcriptional network

Po-Chen Hsu*, Yu-Hsuan Cheng#, Chia-Wei Liao, Richard Ron R. Litan, Yu-Ting Jhou, Florica Jean Ganaden Opoc, Ahmed A A Amine, and Jun-Yi Leu

* Correspondence:

Po-Chen Hsu (godshi2006@gmail.com)

Table of Contents

Appendix Figures

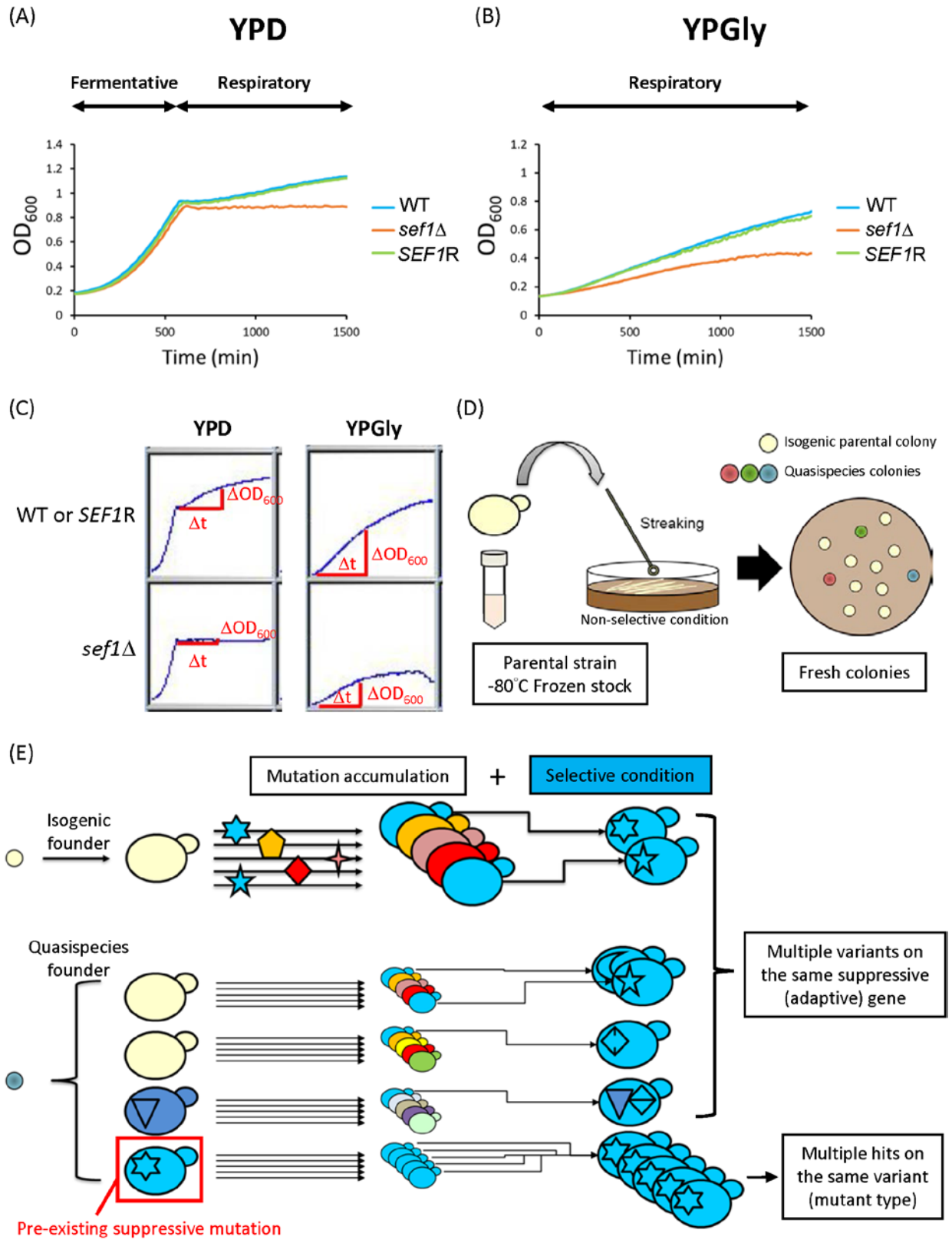

Appendix Figure S1. Deletion of *SEF1* affects fitness and the potential trajectories of

adaptive evolution.

(A) Growth curves of the *sef1*Δ mutant in YPD at 28°C. (B) Growth curves of the *sef1*Δ mutant in YPGly at 28°C. (C) Schematic representation of the maximal slope growth rate calculation for the post-diauxic shift growth phase in YPD and log-phase growth in YPGly. (D) Schematic representation of possible pre-existing genetic variations in the genomes of different individuals in founder colonies. (E) Schematic representation of suppressor formation by selection on pre-existing variations of a quasispecies founder (a population with heterogeneous genomes) or new (*de novo*) adaptive mutations.

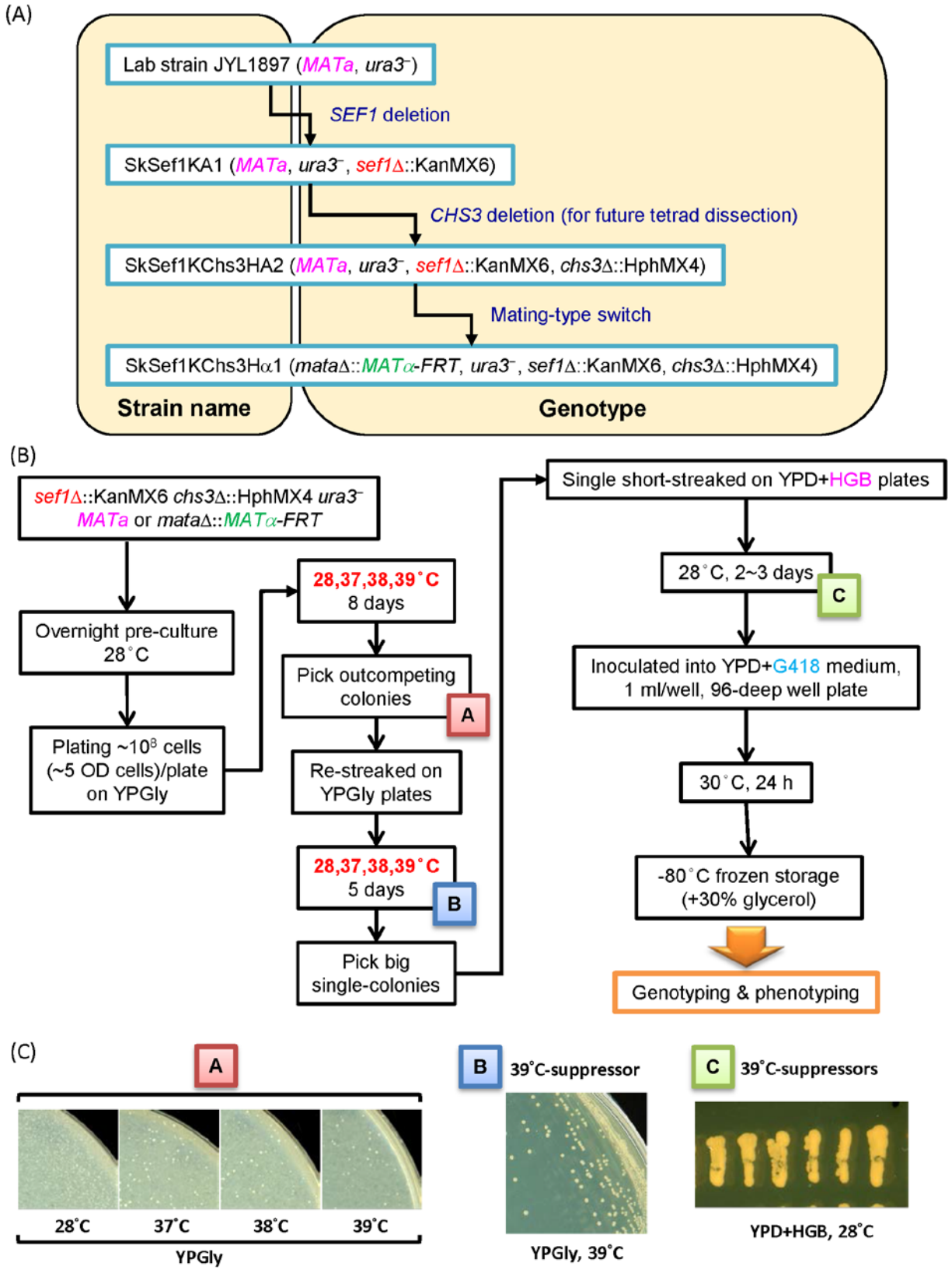

Appendix Figure S2. Workflow of *sef1*Δ suppressor development.

(A) Construction of the *sef1*Δ founder strain. (B) Procedures for *sef1*Δ suppressor

development and selection. (C) Examples of suppressor clone picking and purification steps.

(A)

Total 240 lines

144 MATa lines

96 MATα lines

*sef1*Δ::KanMX6 *chs3*Δ::HphMX4 *ura3*⁻ MATa		
Strain ID	Evolved condition	Strain number
SCHSupr28-01~51	YPGly, 28°C	51 strains
SCHSupr37-01~21	YPGly, 37°C	21 strains
SCHSupr38-01~21	YPGly, 38°C	21 strains
SCHSupr39-01~51	YPGly, 39°C	51 strains

*sef1*Δ::KanMX6 *chs3*Δ::HphMX4 *ura3*⁻ *matα*Δ::*MATα-FRT*		
Strain ID	Evolved condition	Strain number
SCHalphaSupr28-01~33	YPGly, 28°C	33 strains
SCHalphaSupr37-01~15	YPGly, 37°C	15 strains
SCHalphaSupr38-01~15	YPGly, 38°C	15 strains
SCHalphaSupr39-01~51	YPGly, 39°C	33 strains

(B)

Fitness	Score	Category
> WT	5	≥4.5
≈ WT	4	3.5~4.4
> *sef1*Δ, < WT	3	2.5~3.4
= *sef1*Δ	2	1.5~2.4
< *sef1*Δ	1	<1.5

(C)

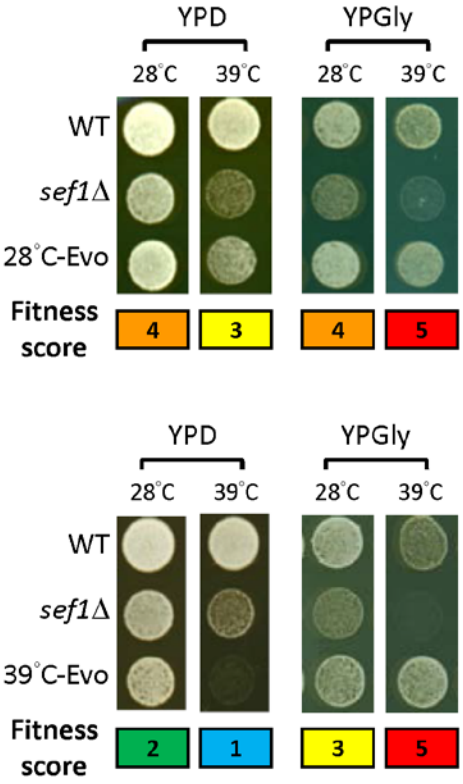

(D)

	YPD				YPGly			
	Fitness score				Fitness score			
Strain	28°C	37°C	38°C	39°C	28°C	37°C	38°C	39°C
WT	4	4	4	4	4	4	4	4
*sef1*Δ	2	2	2	2	2	2	2	2
28°C-Evo	4.0	2.8	2.7	2.8	4.5	3.9	3.6	4.9

Compensation Compensation

(E)

	YPD				YPGly			
	Fitness score				Fitness score			
Strain	28°C	37°C	38°C	39°C	28°C	37°C	38°C	39°C
WT	4	4	4	4	4	4	4	4
*sef1*Δ	2	2	2	2	2	2	2	2
37°C-Evo	2.2	1.4	1.2	1.2	3.1	4.7	4.4	4.9
38°C-Evo	2.0	1.0	1.0	1.0	3.1	4.9	4.9	5.0
39°C-Evo	2.0	1.4	1.2	1.4	3.0	4.7	4.5	5.0

No effect Trade-off Compensation

(F)

	Frequency of inconsistent clones	
	MATa lines	MATα lines
28°C-Evo	2/51 = 3.9%	0/33 = 0%
37°C-Evo	7/21 = 33.3%	2/15 = 13.3%
38°C-Evo	0/21 = 0%	0/15 = 0%
39°C-Evo	1/51 = 2.0%	18/33 = 54.5%
Total	30/240 = 12.5%	

Appendix Figure S3. Summary of 240 *sef1*Δ suppressors.

(A) Descriptions of all suppressors. (B) Criteria for simple fitness scoring and color-specified

categories of *sef1*Δ suppressors. (C) Examples of growth phenotypes and simple fitness scores. (D) Mean simple fitness score of all 28°C-Evo *sef1*Δ suppressors. (E) Mean simple fitness score of all 37°C-, 38°C-, or 39°C-Evo *sef1*Δ suppressors. (F) Frequency of phenotypically inconsistent suppressor clones. Any clone with a simple fitness score higher than the mean score of the same group +1 or lower than the mean score of the same group −1 is defined as an inconsistent clone.

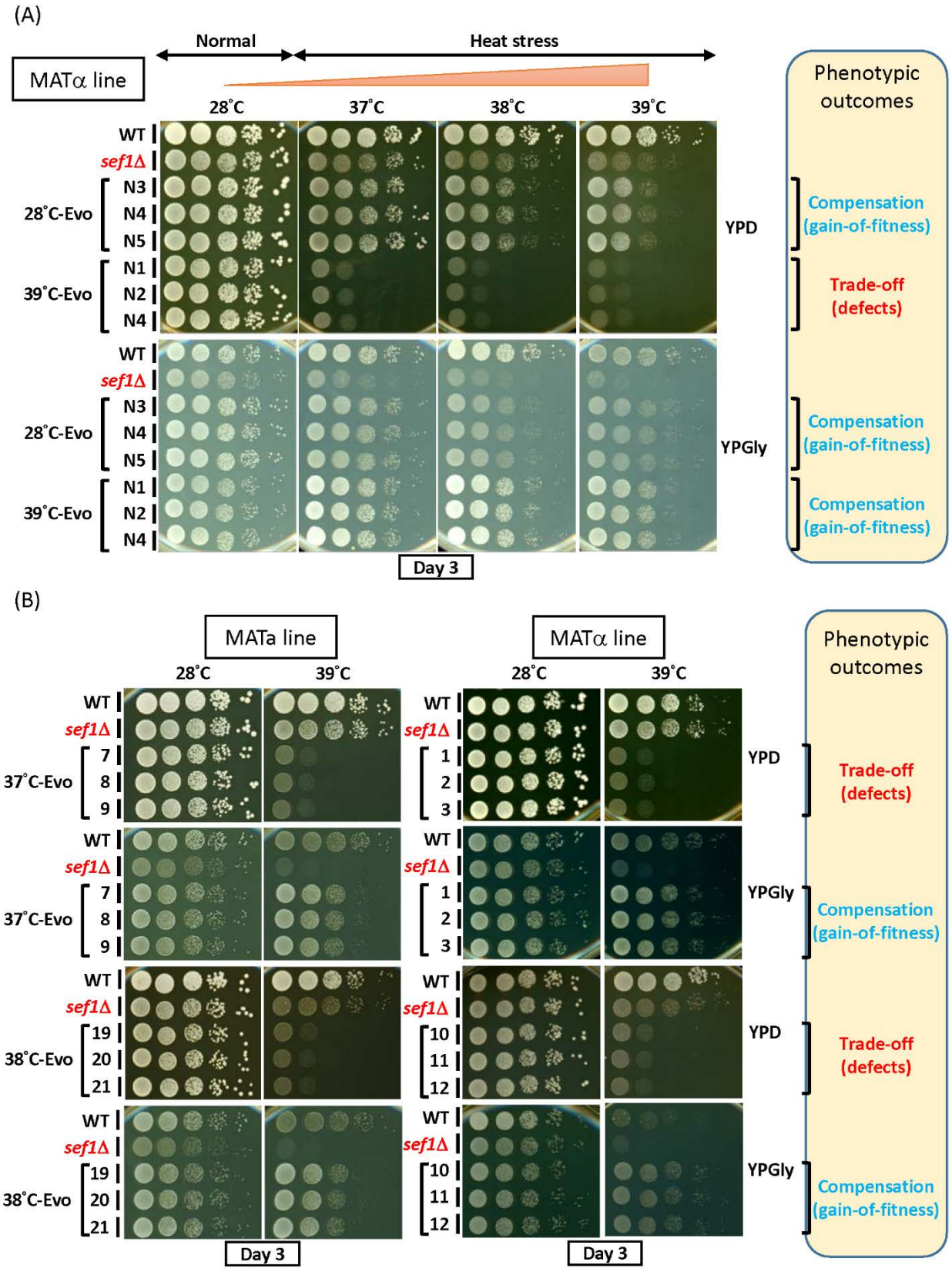

Appendix Figure S4. Phenotypic verification of *sef1*Δ suppressors with consistent

phenotypes.

(A) The suppressive growth phenotypes of re-purified *sef1*Δ suppressor clones (28°C-Evo and 39°C-Evo, MATα line). (B) The suppressive growth phenotypes of other randomly selected *sef1*Δ suppressor clones (37°C-Evo and 38°C-Evo, both MATa and MATα lines).

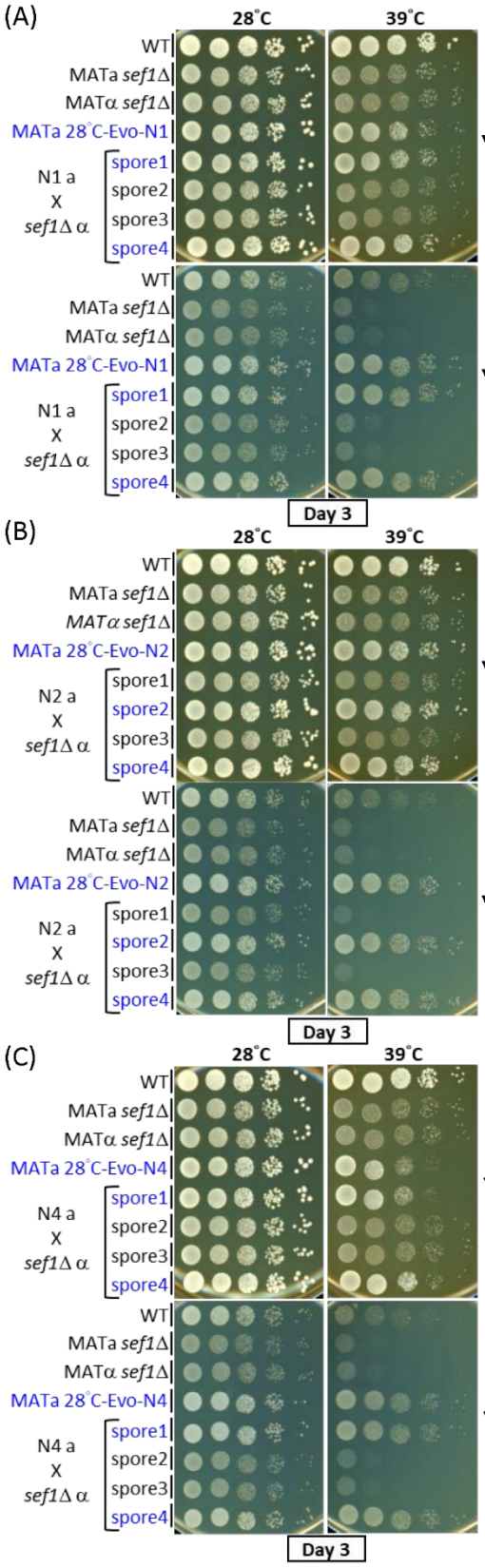

Evo suppressor	Genotype	Note
28°C-N1 MATa	6387_6410del	Mut

Mating	Spore	Genotype	Note
28°C-N1 MATa X *sef1*Δ MATα	1	6387_6410del	Mut
	2		WT
	3		WT
	4	6387_6410del	Mut

Evo suppressor	Genotype	Note
28°C-N2 MATa	5824G>A	Mut

Mating	Spore	Genotype	Note
28°C-N2 MATa X *sef1*Δ MATα	1		WT
	2	5824G>A	Mut
	3		WT
	4	5824G>A	Mut

Evo suppressor	Genotype	Note
28°C-N4 MATa	6387_6410del	Mut

Mating	Spore	Genotype	Note
28°C-N4 MATa X *sef1*Δ MATα	1	6387_6410del	Mut
	2		WT
	3		WT
	4	6387_6410del	Mut

Appendix Figure S5. Genetic dissection of candidate causal mutations in MATa 28°C-

Evo *sef1*Δ suppressors.

Three clones (A) 28°C-Evo-N1, (B) 28°C-Evo-N2, and (C) 28°C-Evo-N4 were dissected. The fitness of spores from each tetrad was examined using spot assays and shown in the left panels. The genotypes of spores from each tetrad were checked by Sanger sequencing and are shown in the right panels. All mutations here are recessive by checking in heterozygous diploid strain (data not shown). Mut – mutant.

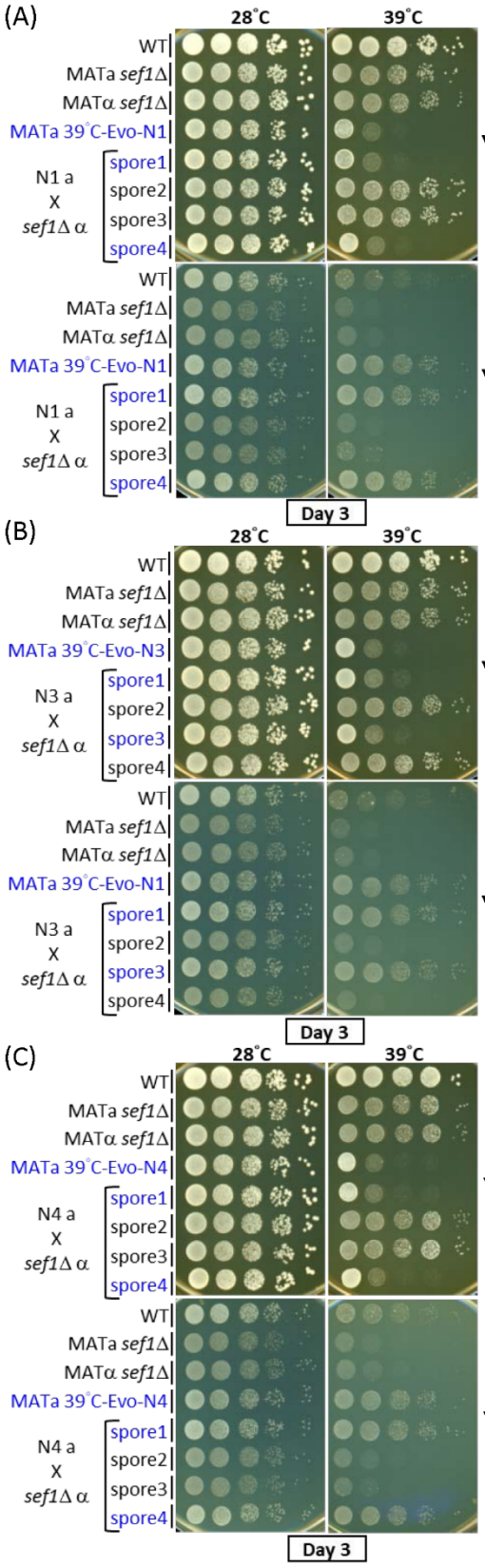

Evo suppressor	Genotype	Note
39°C-N1 MATa	686dupG	Mut

Mating	Spore	Genotype	Note
39°C-N1 MATa X *sef1*Δ MATα	1	686dupG	Mut
	2		WT
	3		WT
	4	686dupG	Mut

Evo suppressor	Genotype	Note
39°C-N3 MATa	1453G>T	Mut

Mating	Spore	Genotype	Note
39°C-N3 MATa X *sef1*Δ MATα	1	1453G>T	Mut
	2		WT
	3	1453G>T	Mut
	4		WT

Evo suppressor	Genotype	Note
39°C-N4 MATa	1453G>T	Mut

Mating	Spore	Genotype	Note
39°C-N4 MATa X *sef1*Δ MATα	1	1453G>T	Mut
	2		WT
	3		WT
	4	1453G>T	Mut

Appendix Figure S6. Genetic dissection of candidate causal mutations in MATa 39°C-

Evo *sef1*Δ suppressors.

Three clones (A) 39°C-Evo-N1, (B) 39°C-Evo-N3, and (C) 39°C-Evo-N4 were dissected. The fitness of spores from each tetrad was examined using spot assays and shown in the left panels. The genotypes of spores from each tetrad were checked by Sanger sequencing and are shown in the right panels. All mutations here are recessive by checking in heterozygous diploid strain (data not shown). Mut – mutant.

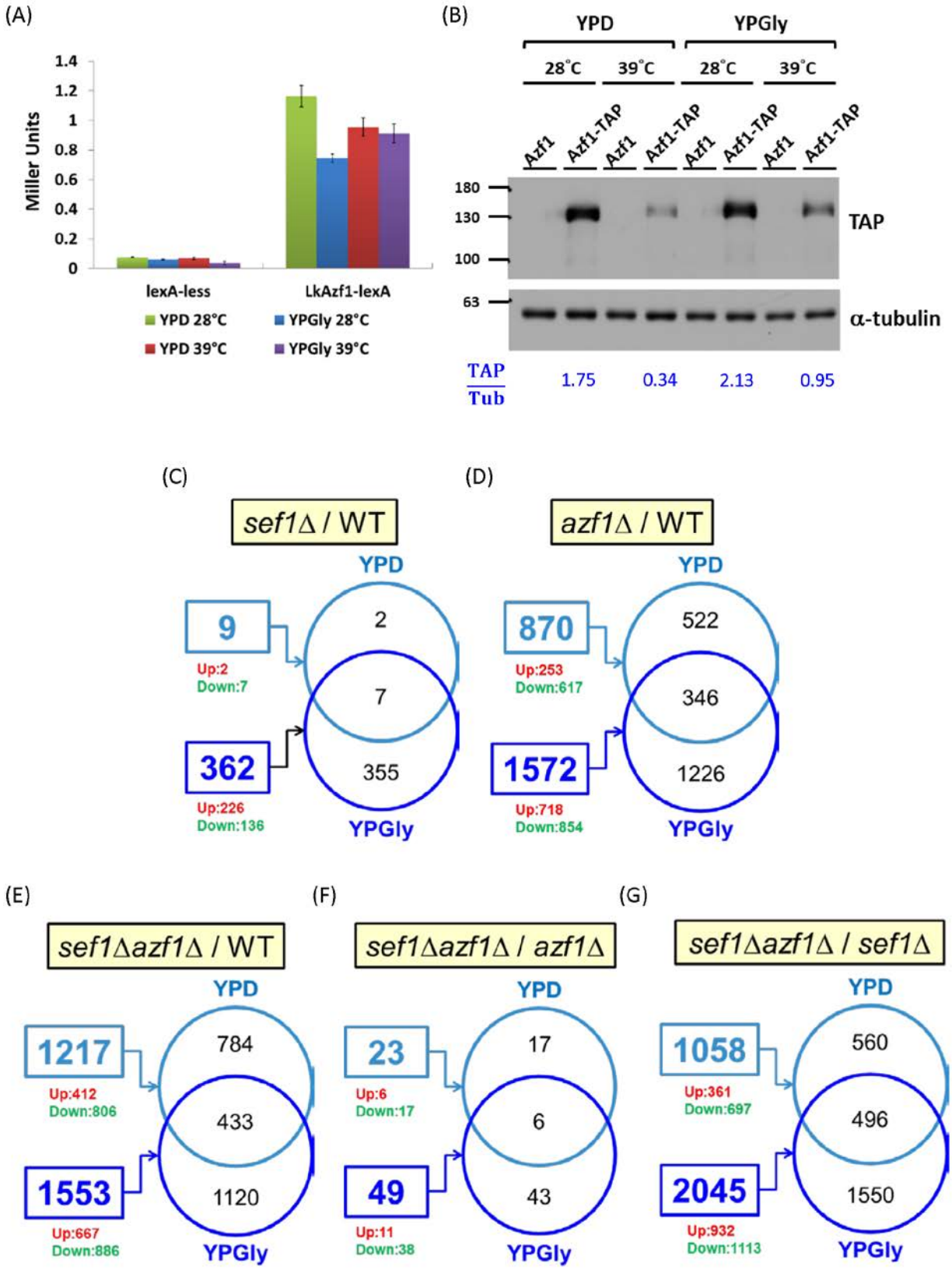

Appendix Figure S7. Differential gene expression in response to *azf1*Δ and *sef1*Δ

mutations.

(A) Heat stress (39°C) slightly reduces the transcriptional activation capability of Azf1, which was measured by one-hybrid assays. LacZ activity was measured by liquid-galactosidase assay and results are displayed as average Miller units ± SD from at least three technical repeats. (B) Azf1 protein abundance is reduced by heat stress (39°C). (C to G) Summaries of numbers of differentially expressed genes in *sef1*Δ/WT (C), *azf1*Δ/WT (D), *sef1*Δ*azf1*Δ/WT (E), *sef1*Δ*azf1*Δ/*sef1*Δ (F), and *sef1*Δ*azf1*Δ/*azf1*Δ (G). Numbers in rectangles are the total numbers of differentially expressed genes under a specific condition. Up or Down: the numbers of upregulated or downregulated genes, respectively. Venn diagrams display numbers of overlapping genes between the two conditions.

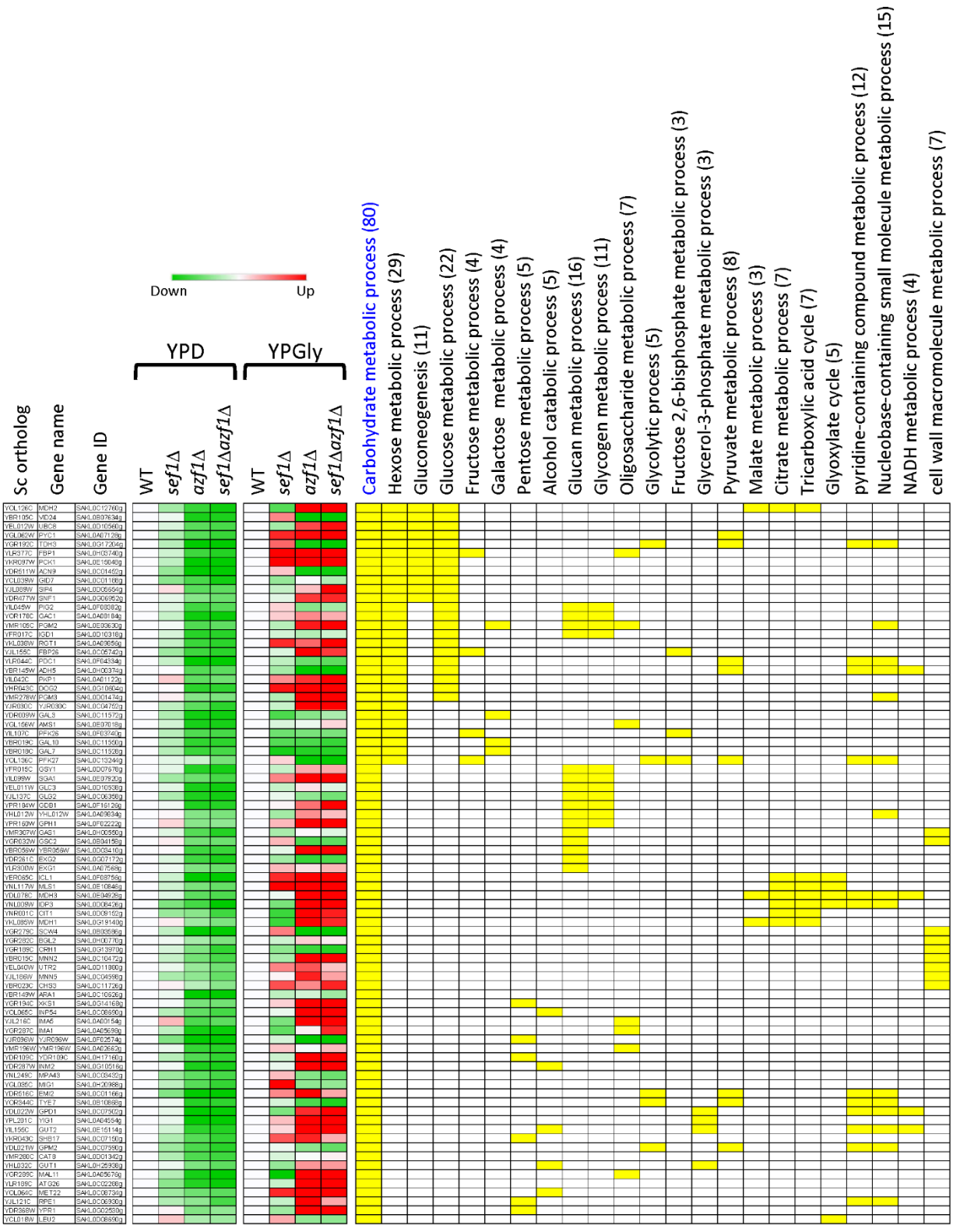

Appendix Figure S8. Dissection of downregulated carbohydrate metabolic process

genes in response to *azf1*Δ mutation under the YPD condition.

The heatmap was generated using the mean TPM ratio from RNA-seq data relative to the wild-type under each condition. The yellow blocks highlight the sub-GO groups to which each gene belongs. Total gene numbers for each GO group are specified in parentheses. The high-resolution source table of the heatmap is provided in Dataset EV17.

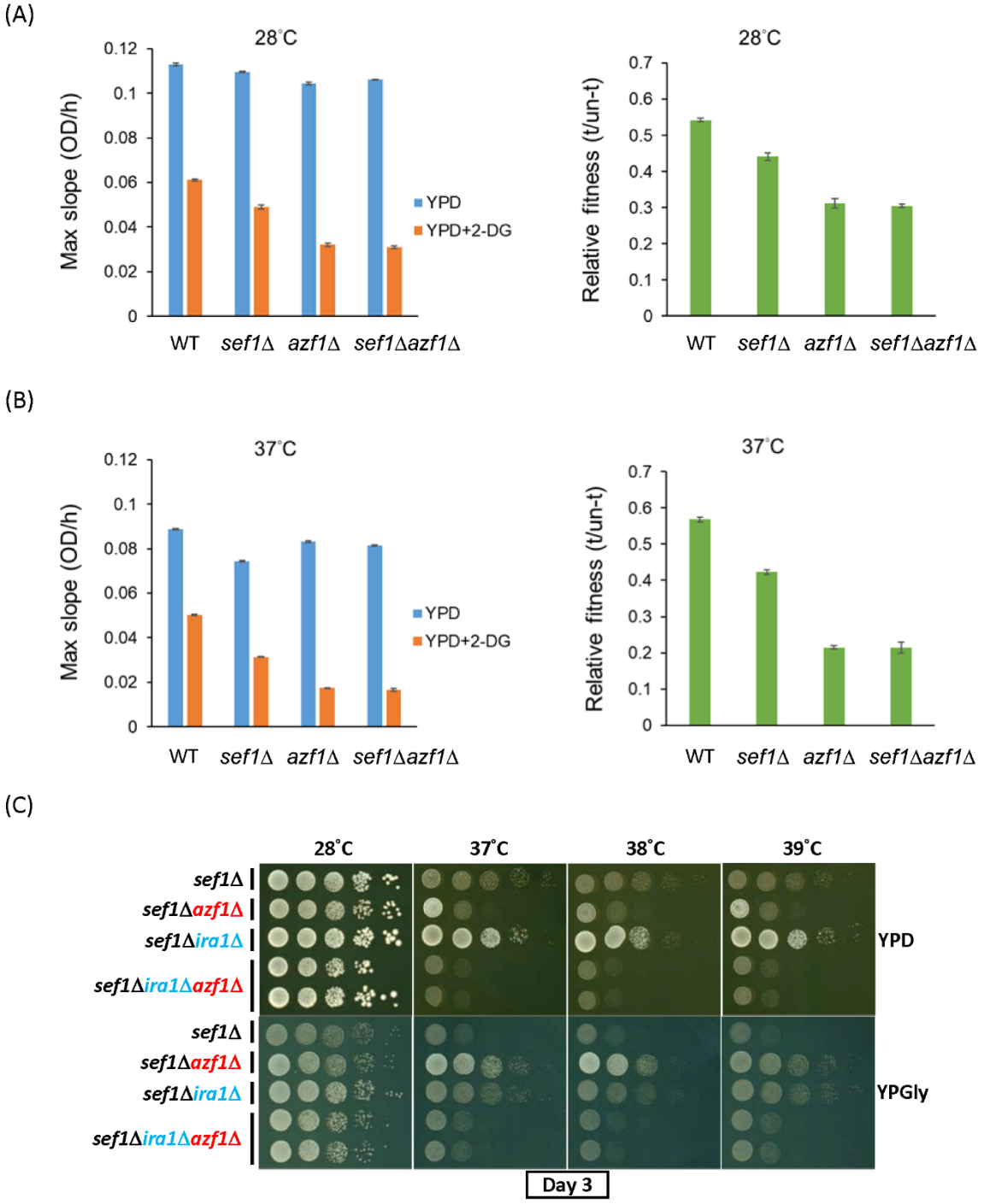

Appendix Figure S9. The fitness of *azf1*Δ cells in response to 2-deoxyglucose under the YPD condition.

(A) Max slope growth rate and relative fitness of the *azf1*Δ mutants at 28°C. (B) Max slope growth rate and relative fitness of the *azf1*Δ mutants at 37°C. For (A) and (B), results are displayed as average max slopes ± SD from three technical repeats. (C) Synthetic growth defect of *azf1*Δ*ira1*Δ in the *sef1*Δ background under heat-stressed conditions.

(A)

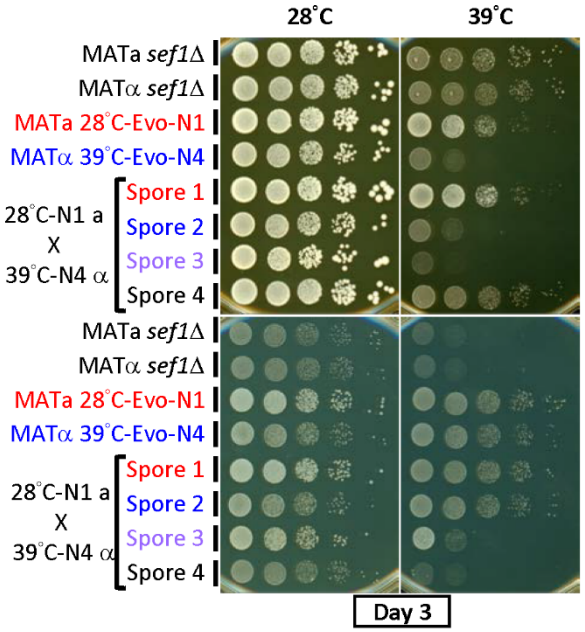

Evo suppressor	Genotype	Note
28˚C-N1 MATa	6387_6410de	*ira1*^{Mut}
39˚C-N4 MATα	686delG	*azf1*^{Mut}

Mating	Spore	Genotype	Note
28˚C-N1 a X 39˚C-N4 α	1	6387_6410del	*ira1*^{Mut}
	2	686delG	*azf1*^{Mut}
	3	6387_6410del 686delG	*ira1*^{Mut} *azf1*^{Mut}
	4		WT

(B)

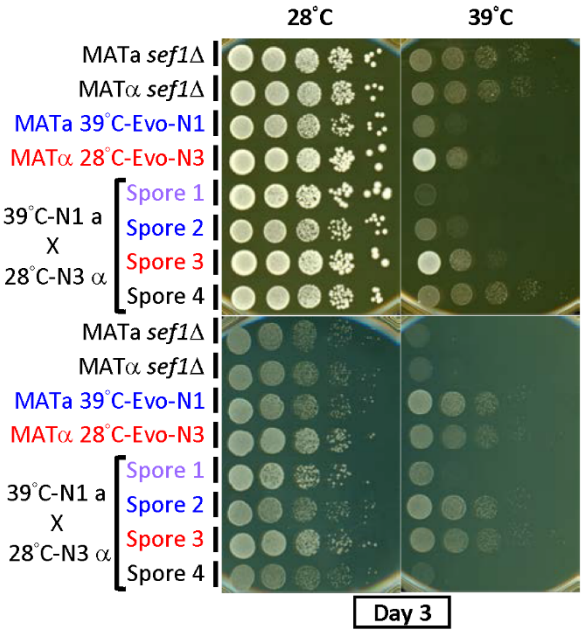

Evo suppressor	Genotype	Note
39˚C-N1 MATa	7098G>A	*azf1*^{Mut}
28˚C-N3 MATα	686dupG	*ira1*^{Mut}

Mating	Spore	Genotype	Note
39˚C-N1 a X 28˚C-N3 α	1	686dupG 7098G>A	*ira1*^{Mut} *azf1*^{Mut}
	2	7098G>A	*azf1*^{Mut}
	3	686dupG	*ira1*^{Mut}
	4		WT

Appendix Figure S10. Synthetic effects of the *ira1* mutation from 28°C-Evo *sef1*Δ suppressors and the *azf1* mutation from 39°C-Evo *sef1*Δ suppressors.

(A) Tetrad dissection and Sanger sequencing of 28°C-Evo-N1 MATa and 39°C-Evo-N4 MATα mating products. (B) Tetrad dissection and Sanger sequencing of 39°C-Evo-N1 MATa and 28°C-Evo-N3 MATα mating products. The fitness of all four spores from each tetrad was phenotyped using the spot assay and shown in the left panels. The genotypes of spores from

each tetrad were checked by Sanger sequencing and are shown in the right panels. The *IRA1* and *AZF1* loci were sequenced.

(A)

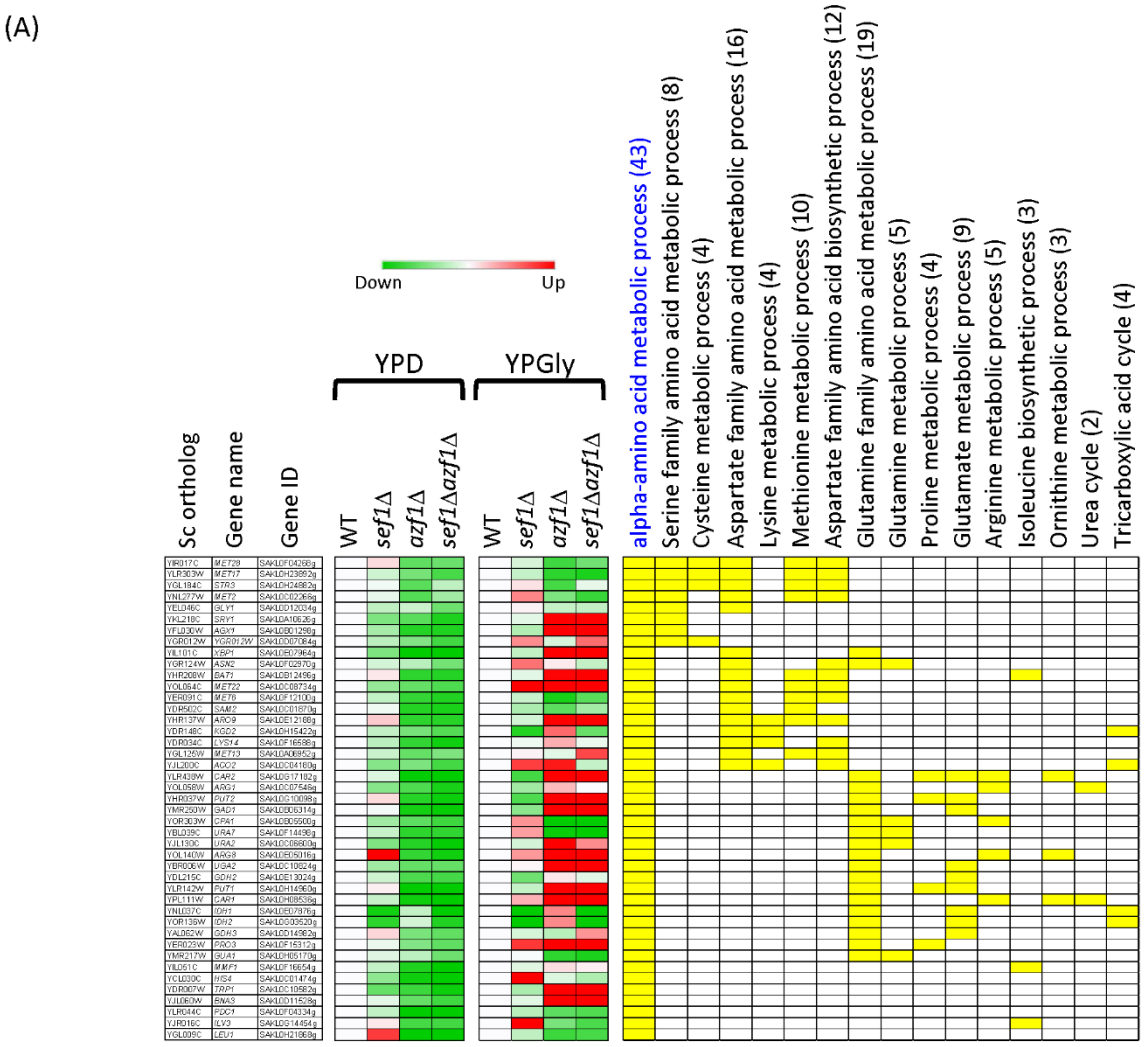

(B)

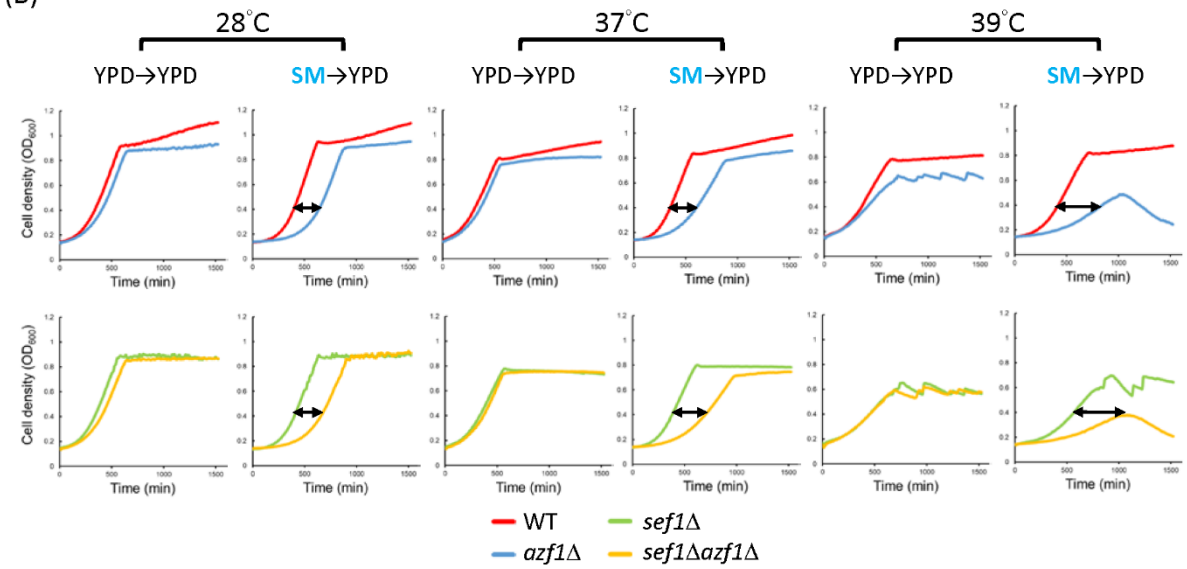

Appendix Figure S11. Dissection of downregulated alpha-amino acid metabolic process genes in response to *azf1*Δ mutation under the YPD condition.

(A) The heatmap was generated using the mean TPM ratio from RNA-seq data relative to the wild-type under each condition. The yellow blocks highlight the sub-GO groups to which each gene belongs. Total gene numbers in each GO group are specified in parentheses. The high-resolution source table of the heatmap is provided in Dataset EV17. (B) The effect of pre-amino acid starvation (23-h starvation in SM+2X uracil medium) on the growth of the *azf1*Δ mutants at indicated temperatures. "YPD→YPD" is the control growth curve without pre-amino acid starvation. "SM→YPD" is the growth curve with pre-amino acid starvation. The jagged curves reflect cellular aggregation or the presence of dead cells mixed with live cells under harsher culture environments. The near-concave curves (39°C, SM to YPD curves) were caused by severe cell death.

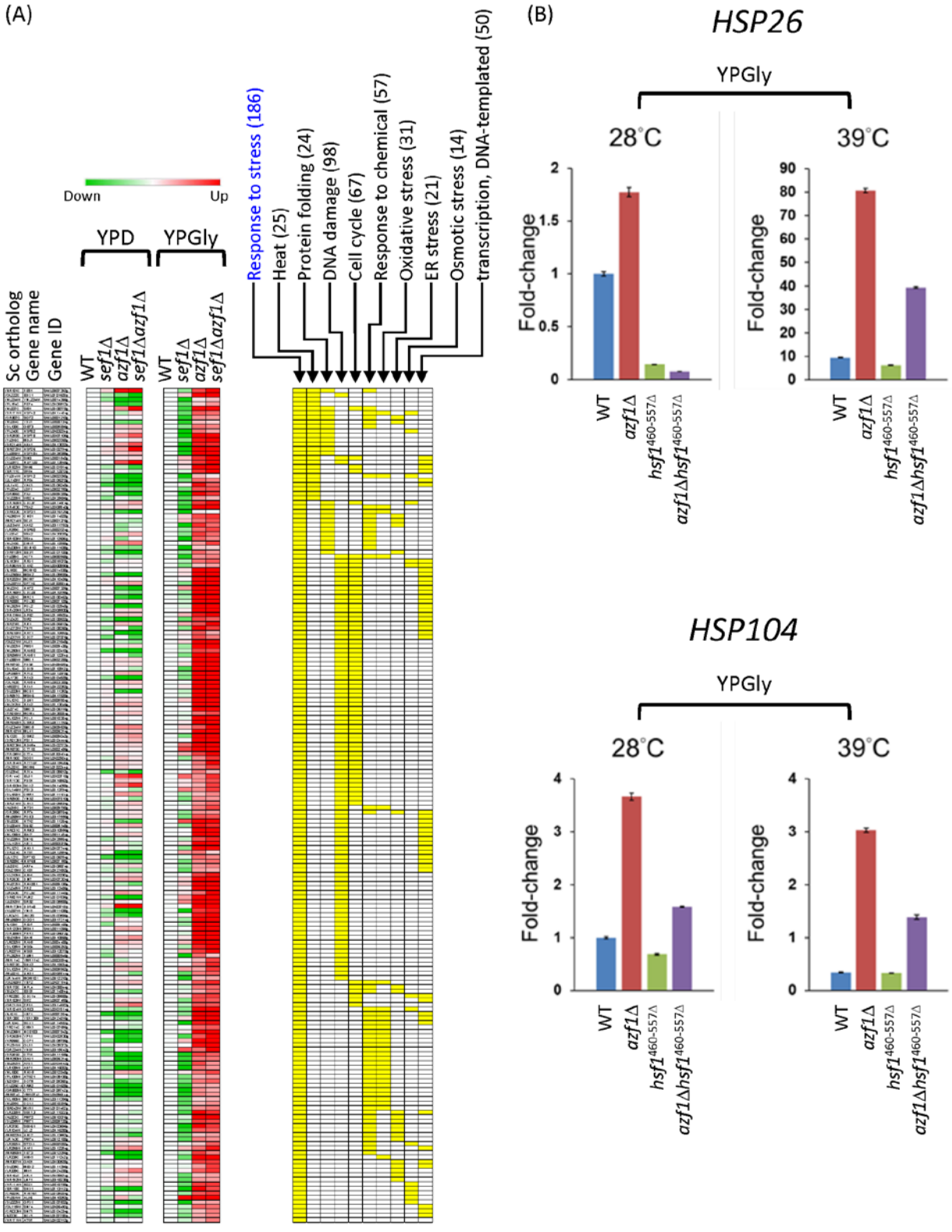

Appendix Figure S12. Dissection of upregulated stress response genes in response

to *azf1*Δ mutation under the YPGly condition.

(A) The heatmap was generated using the mean TPM ratio from RNA-seq data relative to the wild-type under each condition. The yellow blocks highlight the sub-GO groups to which each gene belongs. Total gene numbers in each GO group are specified in parentheses. The high-resolution source table of the heatmap is provided in Dataset EV17. (B) Expression of *HSP26* and *HSP104* in response to hypomorphic *hsf1* mutation (a truncated *hsf1* with the C-terminal 460-557 amino acids removed) under the YPGly condition. The relative fold-change of each gene is shown as $2^{-\Delta\Delta CT}$, using *CDC34* (SAKL0D02530g) as the endogenous control and the ΔC_T value from the wild-type sample as the corresponding calibration value. Expression levels are displayed as mean fold-changes ± SD from three technical repeats.

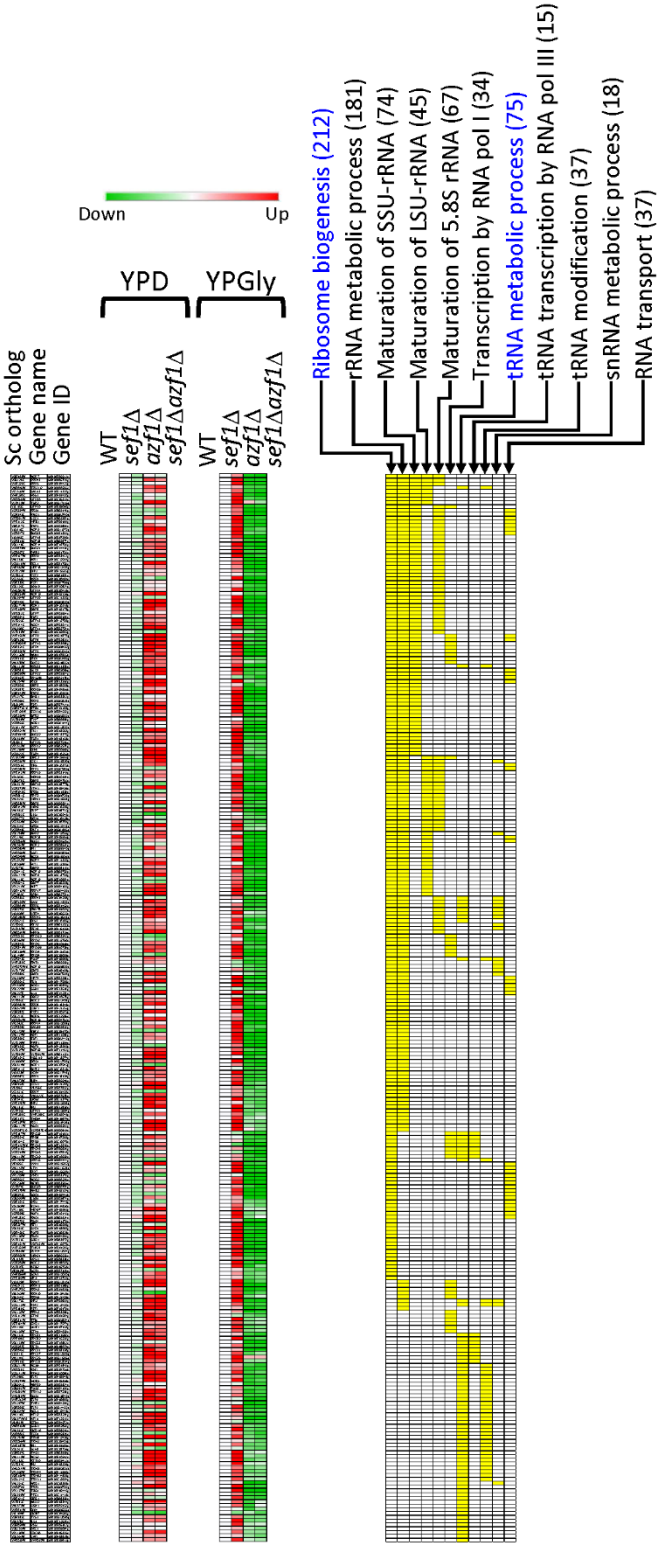

Appendix Figure S13. Dissection of the downregulated ribosome- and tRNA-related

genes in response to *azf1*Δ mutation under the YPGly condition.

The heatmap was generated using the mean TPM ratio from RNA-seq data relative to the wild-type under each condition. The yellow blocks highlight the sub-GO groups to which each gene belongs. Total gene numbers in each GO group are specified in parentheses. The high-resolution source table of the heatmap is provided in Dataset EV17.

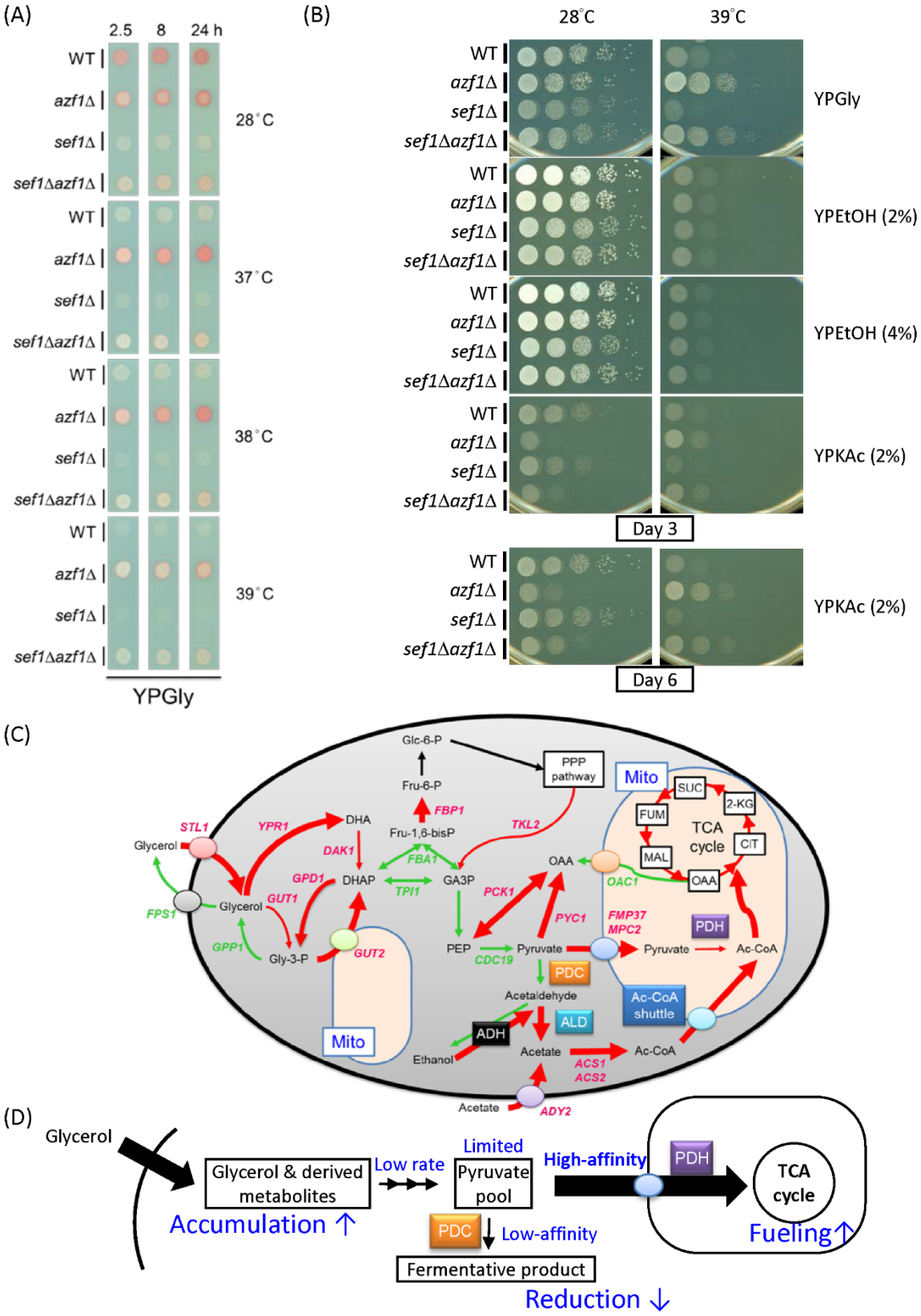

Appendix Figure S14. Glycerol and acetate, but not ethanol, are required for the

enhanced fitness of *azf1*Δ mutants under heat-stressed conditions.

(A) The *azf1*Δ mutants maintain relatively higher TTC reduction activity under the YPGly condition compared to *sef1*Δ strains. The formation of red products in the cell colonies indicates that the cells have competent TTC reduction activity. The whiter spots indicate defects in cellular respiration. (B) Acetate, but not ethanol, endows weaker heat resistance on the *azf1*Δ mutants. YPEtOH (YP + ethanol); YPKAc (YP + potassium acetate). Concentrations of ethanol and acetate are shown in parentheses. (C) Remodeled glycerol utilization in *azf1*Δ cells. Gly-3-P: glycerol-3-phosphate; DHA: dihydroxyacetone; DHAP: dihydroxyacetone phosphate; GA3P: glyceraldehyde-3-phosphate; Glc-6-P: glucose-6-phosphate; Fru-6-P: fructose-6-phosphate; Fru-1,6-bisP: fructose-1,6-bisphosphate; PPP: pentose phosphate pathway; PEP: phosphoenolpyruvate; Ac-CoA; acetyl coenzyme A; PDC: pyruvate decarboxylase complex; PDH: pyruvate dehydrogenase complex; ALD: aldehyde dehydrogenase; ADH: alcohol dehydrogenase; OAA: oxaloacetate; CIT: citrate; 2-KG; 2-oxoglutarate; SUC: succinate; MAL: malate. Mito: mitochondrion. Red arrow: upregulated gene; green arrow: downregulated gene. The thickness of the arrows reflects the relative RNA abundance according to the heatmap presented in Figure 5D. (D) Proposed glycerol-driven metabolic remodeling at the pyruvate node in *azf1*Δ cells. In this model, glycerol accumulates intracellularly due to enhanced uptake, but it is converted to pyruvate at a low rate to maintain a limited pyruvate pool. Consequently, high-affinity mitochondrial pyruvate carriers plus PDH complex compete for the limited pyruvate with the low-affinity PDC complex, thereby fueling respiration rather than fermentation. Accordingly, *azf1*Δ cells benefit from the mitochondrial activity, supporting survival upon encountering heat stress.

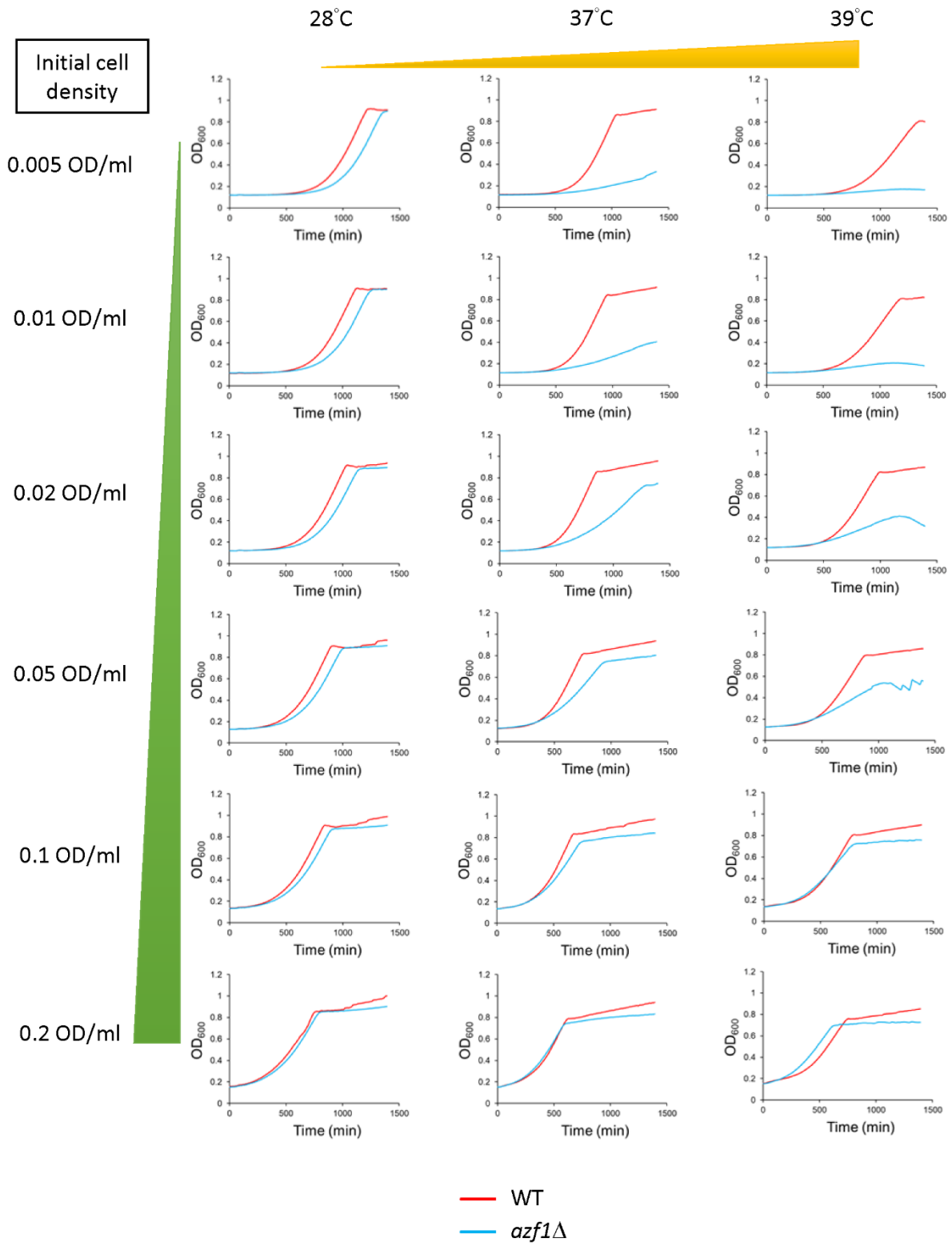

Appendix Figure S15. Growth curves of wild-type and *azf1*Δ mutant cells in YPD in

response to increasing initial inoculum densities and temperature.

Representative source data for Figure 6A.

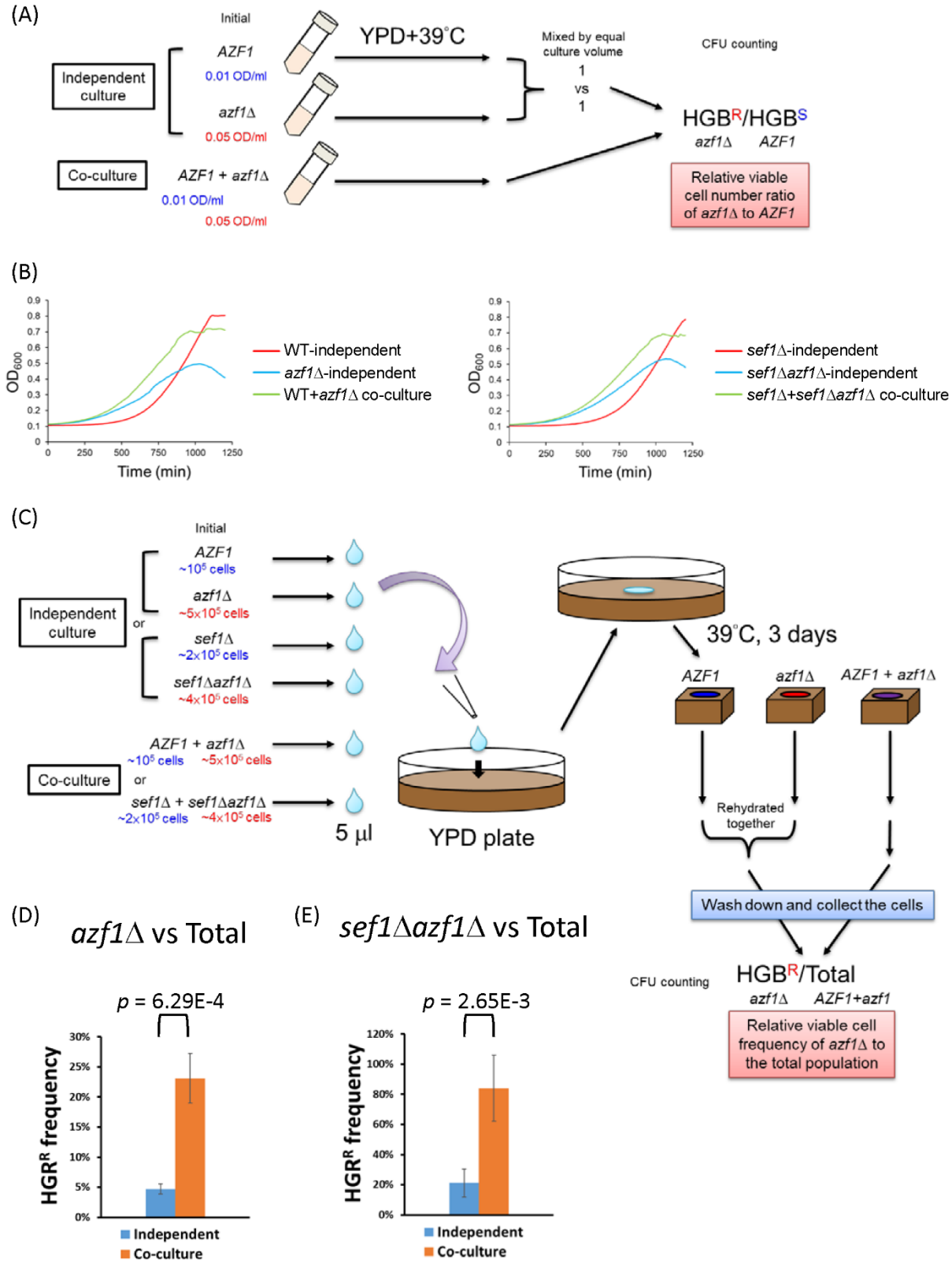

Appendix Figure S16. Cooperative growth assays on the *AZF1* and *azf1*Δ strains.

(A) Illustrative workflow of the cooperative growth assay on the *AZF1* and *azf1*Δ strains in

YPD liquid broth at 39°C. Growth in a 96-well plate was measured on a Tecan plate reader with intermittent shaking. Colony-forming units (CFUs) were counted by plating on YPD (total) and then replicated to a YPD+HGB plate to distinguish HGB-resistant *azf1*Δ strains and HGB-sensitive *AZF1* strains. (B) Source growth curves of Figure 6B and 6C. (C) Illustrative workflow of the cooperative growth assay on *AZF1* and *azf1*Δ strains on a YPD plate at 39°C. (D) The *azf1*Δ cells proved more persistent when co-grown with wild-type cells on an agar plate under the "Dex-trade-off" condition. (E) The *sef1*Δ*azf1*Δ cells proved more persistent when co-grown with *azf1*Δ cells on an agar plate under the "Dex-trade-off" condition. For (D) and (E), results are displayed as average HGB^R/Total ± SD from five technical repeats. Statistical significance tests were carried out using unpaired Student's t-tests.

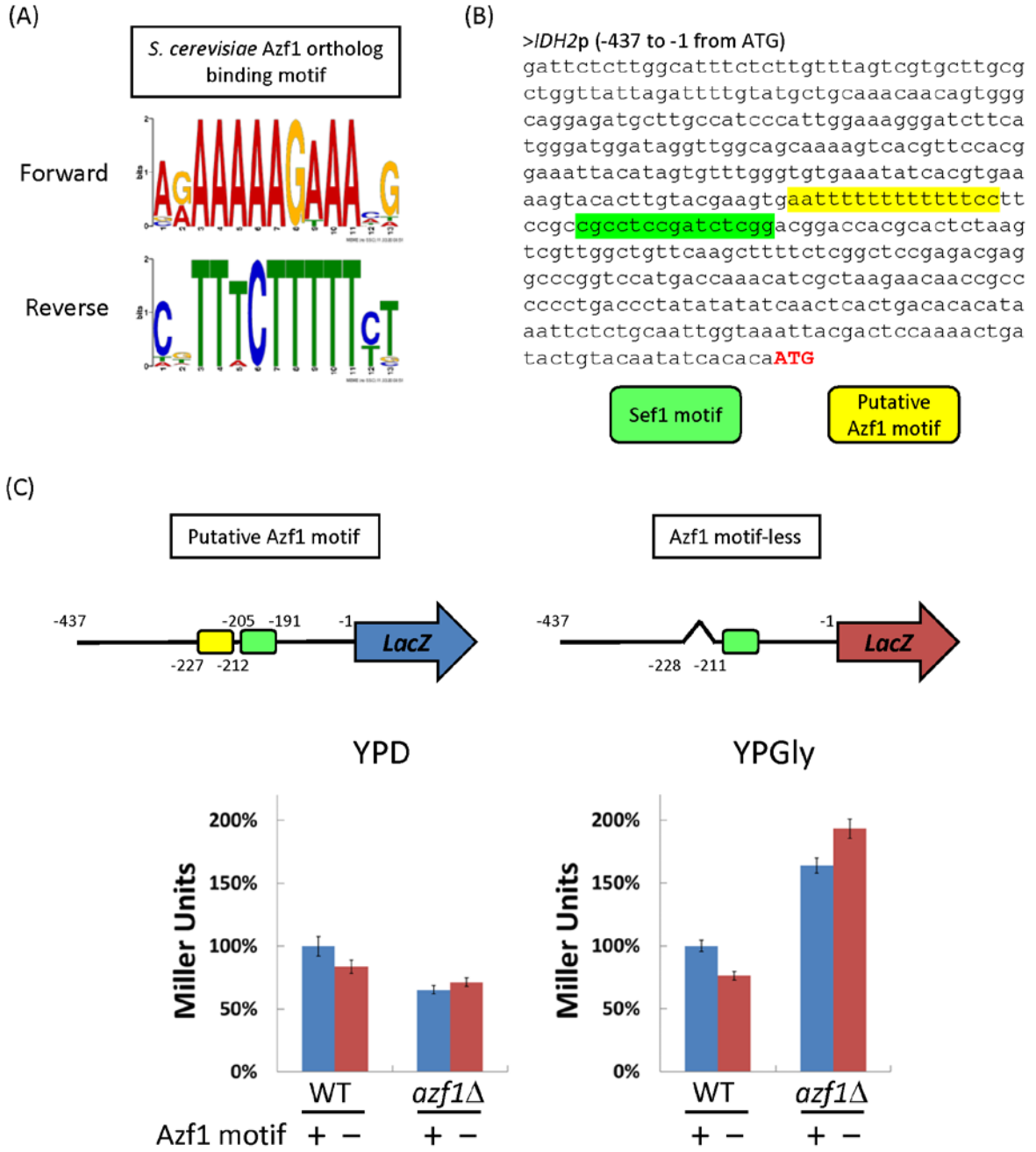

(D)

Gene_Id	log2 Fold change		Sc_Id	Sc ortholog	Functional annotation in Sc
	azf1 Δ / WT	*sef1* Δ*azf1* Δ / WT			
SAKL0F01980g	-2.59	-2.87	YGL209W	MIG2	Zinc finger transcriptional repressor; cooperates with Mig1p in glucose-induced gene repression
SAKL0C10648g	-2.38	-2.12	YPR065W	ROX1	Heme-dependent repressor of hypoxic genes
SAKL0D08734g	-1.42	-1.32	YLR176C	RFX1	Major transcriptional repressor of DNA-damage-regulated genes
SAKL0C05918g	-1.01	-1.81	YKR064W	OAF3	Putative transcriptional repressor with Zn(2)-Cys(6) finger; negatively regulates transcription in response to oleate levels

Appendix Figure S17. Effects of putative Azf1 binding motif on the activity of the *L.*

***kluyveri IDH2* promoter.**

(A) The orthologous binding motif of *S. cerevisiae* Azf1 identified using MEME based on ChIP-exo data in YPD conditions. (B) The *L. kluyveri IDH2* promoter (−437 to −1 from ATG) composed of the entire intergenic sequence and a part of the upstream gene ORF. There are one Sef1 binding motif (−205 to −1191 from ATG) discovered by ChIP-seq and FIMO scanning and one putative Azf1 motif (-227 to -212 from ATG) predicted by FIMO scanning using the orthologous binding motif of *S. cerevisiae* Azf1. (C) The removal of the putative Azf1 binding motif did not reproduce the restoration of *IDH2* expression similar to the effect of *azf1*Δ under the YPGly condition. The *IDH2* expression was measured by the plasmid-based LacZ reporter assays in *L. kluyveri*. LacZ activity was measured by liquid-galactosidase assay and results are displayed as average Miller units ± SD from three technical repeats. (D) The transcriptional repressors downregulated in response to *azf1*Δ and *sef1*Δazf1Δ under the YPGly condition. They are the candidates to cause the restored expression of TCA cycle genes. These candidates were extracted from the total list of downregulated transcriptional regulators in response to *azf1*Δ and *sef1*Δazf1Δ under the YPGly condition (Dataset EV15). The expression data were extracted from the DESeq2 dataset (Dataset EV6 and EV8).

(A)

	Conditions	YPGly, 39°C			
Genotype	MSS Maximum Likelihood Method (MSS-MLE)				
	Mutation Rate (per 10^6)	95% CI range		95% CI median −/+	
		Upper Bound	Lower Bound	Upper Difference	Lower Difference
WT	2.4994	2.7037	2.301	0.2043	0.1983
sef1 Δ	2.1854	2.3655	2.0107	0.1801	0.1747
Genotype	Lea-Coulson Method of the Median Method (LC Method)				
	Mutation Rate Medians (per 10^6)	95% CI range		95% CI median −/+	
		Upper Bound	Lower Bound	Upper Difference	Lower Difference
WT	2.4606	2.673	2.192	0.2124	0.2686
sef1 Δ	2.1854	2.4236	1.8891	0.2382	0.2963

(B)

	Conditions	YPGly, 28°C			
Genotype	MSS Maximum Likelihood Method (MSS-MLE)				
	Mutation Rate (per 10^6)	95% CI range		95% CI median −/+	
		Upper Bound	Lower Bound	Upper Difference	Lower Difference
WT	0.9397	1.0447	0.8388	0.1051	0.1009
sef1 Δ	0.8322	0.9255	0.7425	0.0934	0.0897
Genotype	Lea-Coulson Method of the Median Method (LC Method)				
	Mutation Rate Medians (per 10^6)	95% CI range		95% CI median −/+	
		Upper Bound	Lower Bound	Upper Difference	Lower Difference
WT	0.9397	1.4121	0.6247	0.4724	0.315
sef1 Δ	0.8322	1.0423	0.6118	0.2101	0.2204

Appendix Figure S18. The estimation of suppression rates.

The suppression rates of the wild-type and *sef1*Δ backgrounds under the YPGly condition at (A) 39°C and (B) 28°C. The *sef1*Δ did not result in higher suppression rates than the wild type did, but heat stress (39°C) generally leads to higher suppression rates than at 28°C. Suppression rates (mutation rates) were estimated by using fluctuation analyses from 32 biological repeats. “CI” means confidence interval. The Maximal Likelihood method (the upper panel of each table) and LC method (the bottom panel of each table) generated consistent mutation rates.

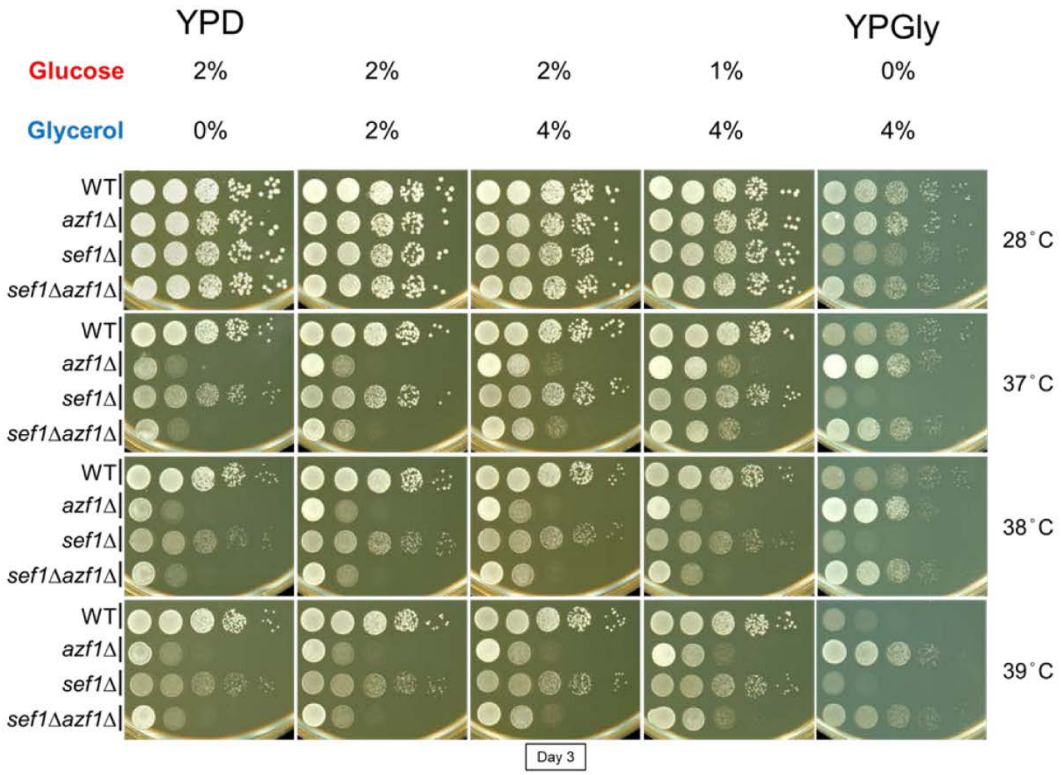

Appendix Figure S19. Effects of mixed glucose and glycerol on growth of *azf1*Δ cells.

Increasing the glycerol concentration in YPD did not drastically ameliorate the "Dex-trade-off" effect. The *azf1*Δ mutants grew slightly better in YPD+4%Gly than in YPD, but still clearly worse than in YPGly. This outcome is possibly due to the protective effect of the elevated osmolarity generated by 4% glycerol.